

From Ground to Aerial Communication: Dissecting WLAN 802.11n for the Drones

Mahdi Asadpour, Domenico Giustiniano, Karin Anna Hummel

Communication Systems Group

ETH Zurich

Zurich, Switzerland

{mahdi.asadpour,domenico.giustiniano,karin.hummel}@tik.ee.ethz.ch

ABSTRACT

Micro Unmanned Aerial Vehicles (UAVs) employed in civil missions are receiving remarkable attention from both research and industry. UAVs embed more and more sensor technology, and their small mounted cameras allow for efficient mapping of large areas in short time. Yet, civil missions such as rescue operations would need a timely delivery of high-resolution images, which calls for high-speed communication such as provided by WLAN IEEE 802.11n. Driven by extensive experiments, the key finding of this contribution is that 802.11n performs poorly in highly mobile and aerial scenarios, as the throughput between UAVs drops far below the theoretical maximum as soon as they become airborne. This is partially caused by the limitations of the embedded hardware, but also a result of the network dynamics of the aerial links. In order to dissect the origins of the low performance figures, we isolate the potential causes of degradation by analyzing our data of throughput, packet loss, aircraft and antenna orientation, and cruise speed. We discuss quantitatively how practical it is to deliver high-resolution images when being exposed to aerial throughput. We believe that it will be a long way until micro UAVs transferring large-size data become reality and argue for a new amendment of IEEE 802.11 addressing the communication among highly-mobile UAVs.

Categories and Subject Descriptors

C.2.1 [Computer-Communication Networks]: Network Architecture and Design—*Wireless communication*

Keywords

Unmanned Aerial Vehicles, IEEE 802.11n, Airborne Wireless Communication, Measurements

1. INTRODUCTION

In civil missions such as Search and Rescue (SAR) operations, micro Unmanned Aerial Vehicles (UAVs) play an

Permission to make digital or hard copies of all or part of this work for personal or classroom use is granted without fee provided that copies are not made or distributed for profit or commercial advantage and that copies bear this notice and the full citation on the first page. Copyrights for components of this work owned by others than ACM must be honored. Abstracting with credit is permitted. To copy otherwise, or republish, to post on servers or to redistribute to lists, requires prior specific permission and/or a fee. Request permissions from permissions@acm.org.

WiTECH'13, September 30, 2013, Miami, Florida, USA.

Copyright 2013 ACM 978-1-4503-2364-2/13/09 ...\$15.00.

<http://dx.doi.org/10.1145/2505469.2505472>.

increasingly important role. As SAR missions are time-critical, UAVs may greatly help the rescue team on the ground by providing a swift first overview of the target area. For instance, state-of-the-art UAVs can carry high-resolution cameras, which can provide an imagery view of the search area and even spot a missing person. Yet, all the potential behind such data is lost if it cannot be delivered to the rescuers in time. As a result, making high-speed communications between flying UAVs is a key challenge in SAR missions.

As cellular network coverage often cannot be assured in case of natural disaster or in wilderness areas such as mountains and forests, SAR missions should best not rely on an infrastructure network, but set-up an ad-hoc network. Making such an approach practical is however far from trivial. Because of cost reasons and limited battery life, UAVs are a scarce resource and only a few UAVs are available to monitor and cover large areas at a given time. This impairs reliable and high throughput communication between UAVs, a problem widely unexplored in related work.

In order to shed some light into this scenario, we conduct an experimental study of the quality of aerial UAV-to-UAV links under varying context parameters. We employ UAVs in a real testbed and make the following contributions by summarizing and extending previous results [3]:

- We introduce a system architecture based on a hybrid network ready for bulk data transfer (Section 3). The networks considered in the hybrid approach are WLAN 802.11n and XBee-PRO 802.15.4. Further, we summarize the implications of embedded hardware restrictions (Section 4).
- By conducting real aerial experiments, we investigate the impact of distance, speed, rate adaptation, and other parameters on link quality and networking performance (Section 5).
- We present an analytical model and estimate the expected aerial transmission time for large-size image data transfer (Section 6).

We show that UAV-to-UAV 802.11n throughput drops far below the theoretical maximum and just reaches throughput at the level of the older 802.11a/g technology, despite novel 802.11n features such as transmit spatial coding, channel bonding, and frame aggregation. We investigate potential causes and their impact in isolation. Key conclusions are that the 802.11n automatic rate adaptation cannot cope

with highly mobile and dynamic wireless channels. Additionally, we find that the interplay of the Doppler effect and the antenna direction causes high packet losses across different relative speeds and positions.

2. RELATED WORK

Micro flying robots, also termed drones or UAVs, are nowadays equipped with small on-board cameras. Such cameras can be used to: (i) enable autonomous flight of UAVs by using on-board computer vision algorithms [12], and (ii) take pictures that are processed after landing in order to create a 3D map [10]. An image collection like that is, however, not suitable for SAR missions since the rescuers urge to visually inspect the pictures right away, with the least delay possible.

UAVs are also leveraged as communication supporters in different mission contexts. In principle, UAVs may act as relays [19], as known in other multi-hop wireless networks, or as ferries [8,9] leveraging own mobility to transmit data between remote stations through air-to-ground links. Hereby, commercial off-the-shelf wireless devices are economically preferred, such as WLAN operating in 802.11a mode [17].

However, UAV networks are challenged by the dynamics of movement, which have not been considered so far by traditional wireless networking approaches designed for stationary or low mobility contexts, such as mesh networks [2,16]. Networking is affected as signal propagation changes frequently and protocols have to adapt for optimizing link quality assessment, PHY rate selection, and antenna orientation in 3D space. In case of high speeds, also the Doppler effect has to be considered. The significant influence of antenna orientation is discussed in [18] for air-to-ground links in terms of achievable throughput and number of retransmissions in the 5 GHz frequency band. A limitation of previous works is that they have not addressed the air-to-air link, which we aim to characterize in this contribution.

Finally, the high throughput of classical wireless network deployments is also desired in UAV networks. Yet, high-speed delivery of bulky data requires a physical layer, such as provided by 802.11n [1], that can support high data rates. Wi-Fi 802.11n has been extensively studied in indoor environments [13,15], but it has received little attention in aerial communication. With our work, we aim at closing this gap.

3. SYSTEM ARCHITECTURE

In an SAR scenario, UAVs aim at finding a missing person within a predefined area with minimal delay by deploying a fleet of UAVs and possibly other agents.¹ As depicted in Figure 1, the area is separated into sub-areas termed ‘cells’, with each cell of size A_{cell} . A cell is scanned by a UAV taking images of different parts of this cell. The size of the area covered by an image is termed A_{image} . The ‘planner’ resides at the ground station and calculates plans to efficiently coordinate the mission by taking the environment into account such as wind and weather conditions, terrain information (irregularity level, clutter level, etc.), and online input from UAVs. In particular, the mission planner controls the UAVs and their movement, and receives in return location information, such as GPS positions, and other sensory information from the UAVs [5].

¹The cooperation of heterogeneous search agents is, e.g., addressed by our SWARMix approach; more information can be found at <http://www.swarmix.org/>.

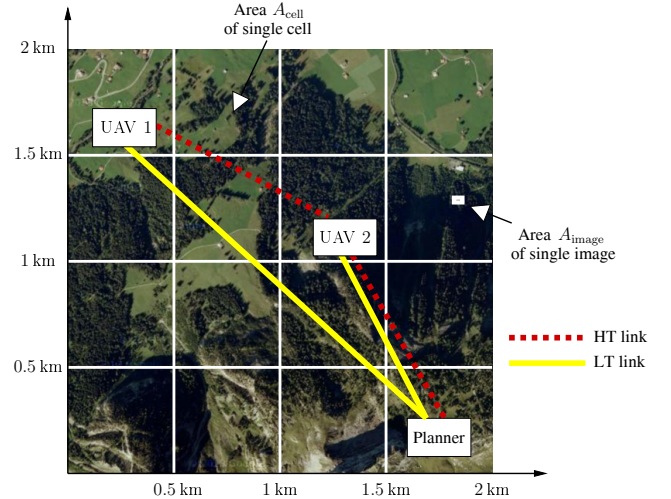


Figure 1: Hybrid communication network ready for image transfer (HT=High Throughput, LR=Long Range): one UAV (UAV 1) scans a cell and transfers image data via another UAV (UAV 2) to the ground station (planner) leveraging the HT network. In addition, the LR network maintains the control channel between each UAV and the planner.

UAVs are equipped with high-resolution cameras but also with multiple sensors such as wind and acceleration sensors, and wireless communication technologies to report to the planner and to receive instructions from the planner. On the one hand, status information and commands demand only low throughput but reliable links, and on the other hand transferring images or videos demands high throughput links. Thus, we propose a hybrid system that leverages two different networks: a ‘long range’ (LR) wireless network such as XBee, cellular if available, or a network utilizing white space frequencies, and a ‘high throughput’ (HT) wireless network such as WLAN IEEE 802.11. To increase the range of the HT network, UAVs build an ad-hoc multi-hop wireless network termed Unmanned Aerial Network (UAN). Because of cost reasons, it is currently unrealistic to deploy a high number of UAVs. Therefore, the UAN is partially disconnected, and communication distance varies over time according to the position (cell and actual position) of the UAVs.

3.1 Image Data

High-resolution images of the cells are sent using the UAN. At the planner, computer-vision processing is performed. This is advantageous, as, albeit partial image processing can be done by the UAV’s on-board micro-controller [12], this would further drain the UAV battery. Besides, the planner can take better decisions, if aware of the entire collected data, and the human expert still can stay in control by sighting the raw image material.

Each cell is scanned by one UAV using a mounted camera with resolution of $R_{\text{px}} \times R_{\text{py}}$ [pixel]. The resolution must be selected as a trade-off between detection possibility and network load caused. Using appropriate different compression techniques will result in different file sizes, M_{image} [bits]. Further, each picture covers an area A_{image} . A picture taken

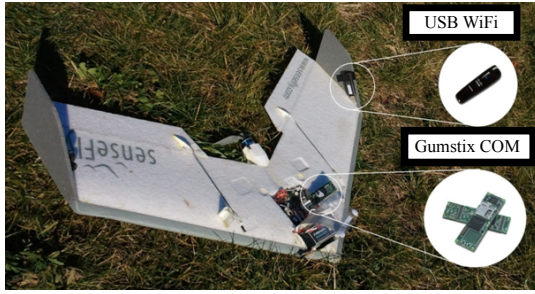


Figure 2: The UAV/swinglet.

by a typical camera is rectangular with an aspect ratio k , and the Field Of View (FOV) is the diagonal of the rectangle. Therefore, by changing altitudes, UAVs can change the size of their observation areas [4]. Hence, the covered area is calculated as:

$$A_{\text{image}} = \left(k \times \frac{\text{FOV}}{\sqrt{k^2 + 1}} \right) \times \left(\frac{\text{FOV}}{\sqrt{k^2 + 1}} \right).$$

The cell is scanned with approximately $A_{\text{cell}}/A_{\text{image}}$ images. Finally, the total amount of data M_{cell} to be communicated through the UAV-to-UAV link is given by:

$$M_{\text{cell}} = \frac{M_{\text{image}} \cdot A_{\text{cell}}}{A_{\text{image}}}. \quad (1)$$

4. SYSTEM IMPLEMENTATION

Deploying a network of UAVs capable of disseminating high-resolution images of an area in a real setting requires the selection of an appropriate, light-weight flying platform and wireless communication modules.

4.1 Flying Platform

We employ ‘swinglets’, that are, light-weight fixed wing UAVs developed at the Laboratory of Intelligent Systems at EPFL [11] (see Figure 2). The UAV has a wingspan of 80 cm and a small weight (total weight is approximately 500 g including a small mounted camera). An electrical motor drives its single propeller and enables flying. A lithium polymer battery is used that provides flight autonomy of more than 30 minutes. The UAV’s cruise speed is 10 m/s and the altitude reached is more than 400 m. The main parameters are summarized in Table 1.

The main electronic system of the UAV is the autopilot, which integrates a GPS unit, pressure sensors, and inertial sensors. The autopilot enables the UAV to take off and land autonomously and to navigate through defined way-points. Way-points can be set through a graphical user interface

Table 1: Swinglet parameters.

Nominal endurance	30 min
Cruise speed	10 m/s
Typical climbing speed	3 m/s
Max wind speed	7 m/s
Minimum turning radius	20 m
Typical altitude range	20 – 500 m

on the ground station. The communication link from the ground station (planner) to every UAV is based on an XBee-PRO 802.15.4 radio operating in 2.4 GHz frequency band, which provides low bandwidth (only up to 250 kbps) but long range (up to 1.2 km). The XBee network is used for control messages and short sensor and status information, yet, it is not appropriate for transferring bulk data such as images. A detailed electronic specification of the swinglet can be found in [11].

4.2 WLAN 802.11 Communication

The UAV is further equipped with a WLAN 802.11n module. For this purpose, the original UAV platform is extended by a Gumstix Overo Tide computer-on-module running a Linux distribution and residing next to the autopilot. The 802.11n USB dongle is attached with the help of an expansion board.

We select a Linksys 802.11n USB dongle with Ralink 3572 chipset due to its Linux compatibility, dual 2.4 and 5 GHz bands capability, light-weight design (weight: 11 g, dimensions: 79.9 × 25.4 × 12.4 mm), and the flexibility of its driver which allows to configure various parameters including the PHY rate. The dongle is integrated into the left wing of the UAV as marked in Figure 2, as the noise generated by other on-board electronic components is less disturbing when selecting this placement. The card integrates two planar antennas and operates with the recent 802.11n amendment of IEEE 802.11, which exploits Multiple Input Multiple Output (MIMO). At boot up, UAVs establish an ad-hoc connection with each other and the planner at channel 40 in the 5 GHz band. We operate in the 5 GHz band to avoid interference with the XBee network operating in 2.4 GHz band.

4.3 Implications of the Implementation

The UAVs employed have some advantageous characteristics as they are light-weight and, thus, cause limited safety problems in case of crash failures. Further, they are capable of flying at high altitudes and at high speeds. On the downside, the limited weight comes with limited freedom to apply communication modules without endangering the flying functions, which challenges high-speed communication:

- The embedded hardware required to stay light-weight and support flight functions, causes limited capabilities in terms of CPU power, storage, and available off-the-shelf 802.11n communication modules.
- Although it is known that antenna characteristics and orientation strongly impact networking quality [18], mounting external antennas on a UAV is constrained by the antenna weight and possible disturbances of flight functions.
- Finally, all wireless networking functions and protocols implemented in available driver software are exposed to ongoing high-speed movement and resulting variations of signal quality.

Given these challenges and principle limitations, we want to answer the question whether high throughput 802.11n UAV-to-UAV communication is practical and to what extent high resolution images can be delivered over these aerial links. In the next section, we investigate this problem by experimentally studying the quality of the aerial UAV-to-UAV links.

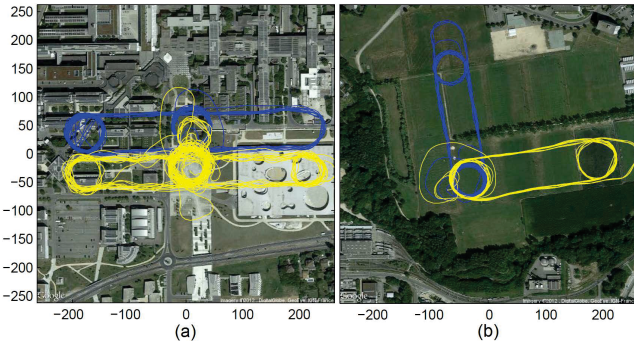


Figure 3: GPS traces collected during the experiments with two UAVs when (a) they approach each other and depart, and (b) they fly towards a meeting point. During the flying activity, we measure 802.11n throughput, packet loss, RSSI, and other parameters.

5. EXPERIMENTS

We conduct real experiments comprising two UAVs and a laptop. In the tests, 802.11n features are enabled. Among others, the main features we use are MIMO PHY layer, channel bonding, frame aggregation, and block acknowledgment [1]. Our tests aim to assess the quality of aerial 802.11n links and to evaluate the impact of distance, relative speed, antenna orientation, and PHY rate adaptation on packet loss and throughput. To do so, we log the following data once per second:

- UAV parameters: current GPS position (latitude, longitude, altitude), altitude via pressure sensor, ground speed, battery level, etc.
- Communication parameters: throughput, packet loss, RSSI (Received Signal Strength Indicator, for two antennas), SNR (Signal to Noise Ratio, again for two antennas), etc.

5.1 Test Scenarios

Each of the two UAVs is configured to fly between two distinct points for a couple of minutes. As our UAVs do not support automated collision avoidance, we configure them to follow waypoints at different altitudes: 80 and 100 m, respectively. Hence, the UAVs can approach one another as close as desired without colliding. We generate UDP traffic at different rates using *iperf* and perform throughput measurement of data transmissions between the flying UAVs.

Our test scenarios are:

- **Scenario A:** To reach high relative speeds, the two UAVs' waypoints are set to fly towards and away from each other, as depicted in Figure 3(a). In this scenario, the *iperf* data rate is set sufficiently high, that is, 80 Mb/s, to evaluate the maximum UDP throughput achievable through UAV-to-UAV links with dynamic channel conditions.
- **Scenario B:** In this scenario, one UAV is configured to fly straight back and forth towards a meeting position, and the other UAV moves perpendicularly to

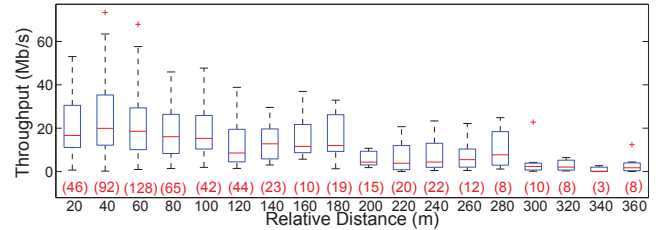


Figure 4: Throughput vs. relative distance for Scenario A.

this movement. The GPS traces are depicted in Figure 3(b). During the test, the UAVs are roughly synchronized w.r.t. moving along the meeting circle. As a result, the relative speed is often less than their individual ground speeds. In this scenario, *iperf* sends at a data rate up to 30 Mb/s and we evaluate the impact of packet losses and PHY rate on the measurements.

In both scenarios, the 802.11n USB dongle is always placed into the left wing of each swinglet (see Figure 2). Thus, by investigating different pathways, we can further analyze the influence of the antenna positions relative to one another on the received signal quality.

5.2 Results

In the following, we present the throughput and packet loss rate experienced, and investigate potential causes of performance drop with respect to our expectation. The results are visualized as boxplots showing median, 25% and 75% quartiles, and extreme values. Numbers in parentheses give the number of samples available for evaluation.

5.2.1 Impact of Distance

As reference scenario, we measure the throughput in an indoor environment using laptops and our 802.11n chipsets. A UDP throughput of up to ≈ 176 Mb/s is achieved using 802.11n which agrees with findings in related work [13]. Next, we show that this throughput is not obtained via aerial links between UAVs.

Figure 4 shows the throughput versus distance for Scenario A, where the distance is calculated applying the Haversine formula to GPS coordinates. The median of throughput shows a degradation along increasing distance. In addition, the throughput shows high variability even for short distances. At short distances, the throughput (≈ 19 Mb/s) is similar to the one expected of 802.11a/g implementations (i.e., ≈ 24 Mb/s), but is significantly lower than the one expected of 802.11n (i.e., up to ≈ 176 Mb/s). The lack of sufficient spatial diversity of the aerial UAV-to-UAV channel limits any exploitation of the 802.11n multiple antennas. Yet, one would expect that other 802.11n protocol features such as channel bonding, frame aggregation, and block acknowledgment should still allow us to achieve higher throughput. In the following we investigate potential causes including Doppler effect, antenna orientation, and automatic PHY rate.

5.2.2 Impact of Relative Speed

In order to evaluate the impact of the relative speed on the losses, we investigate the Packet Delivery Ratio (PDR) as a function of the relative speed between UAVs for Scenario A.

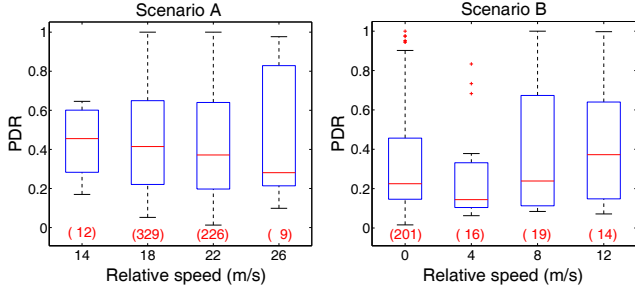


Figure 5: PDR vs. relative speed.

nario A and B (see Figure 5). Because of the noise in the reported relative speed, we group the raw samples into bins with similar speed.

Inspecting the results of Scenario A, we observe intermediate losses across the entire range of speed values. We claim that at high relative speeds between two moving UAVs, transmission degradation due to Doppler effect is expected. The reason is that the Doppler shift correction in the preamble is assumed to be valid for the entire packet, which may cause packet losses when the coherence time is equal to or smaller than the packet duration [7].

In order to study the impact of Doppler in the tests, we can consider that the UAVs' relative motion causes a Doppler shift of $\frac{f_c \cdot \Delta v}{c}$, where $f_c = 5.2$ GHz (channel 40) and c is the speed of light. For a relative speed of $\Delta v = 15$ m/s, we have a coherence time of $1/(4 \cdot \text{Doppler shift}) = 0.96$ ms [14]. On the other hand, the 802.11n A-MPDU frame aggregation is designed to amortize the channel contention by using the principle that multiple subframes of the A-MPDU are transmitted in one frame of up to 64 KB and using one single PHY preamble [1]. The duration of this A-MPDU frame is likely longer than the coherence time of 0.96 ms. For instance, without considering the protocol overhead, 64 KB can be transmitted at 100 Mb/s in a time longer than 5.2 ms, hence causing a burst of losses.

We then evaluate how the relative speed impacts the PDR in Scenario B, where lower relative speed is achieved by choosing different flight trajectories (see Figure 3). The results are summarized in Figure 5. More than 80% of the samples are available for a relative speed between 0 and 2 m/s (all grouped in the bin at speed 0 m/s.). Despite the lower relative speed, the PDR is even lower than for Scenario A, with median PDR of ≈ 0.2 . The conclusion of both scenarios is that the median PDR is dramatically low across all ranges of values and that the Doppler effect can not explain (alone) the low observed PDR.

5.2.3 Impact of Trajectory and Antenna Position

In the following, we assess whether the waypoints of Scenario A and B (Figure 3) affect the observed PDR. Further, we study whether this can explain the lower PDR for Scenario B when compared to Scenario A, despite the lower relative speed. To this end, we investigate the RSSI and the SNR. We plot the results in Figure 6 (Scenario A) and Figure 7 (Scenario B) for each of the two internal antennas of the 802.11n transceiver. As shown in Figure 8, antennas are mounted on the left wing of each UAV. They change their relative position to one another depending on the trajectory. In Scenario A, the orientation assures almost line-of-sight

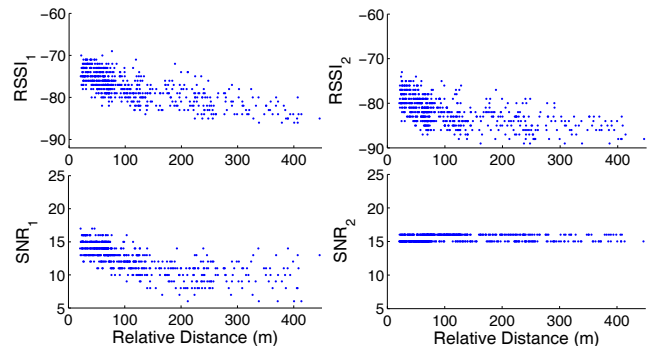


Figure 6: RSSIs and SNRs, for antenna 1 (left) and 2 (right), vs. relative distance for Scenario A.

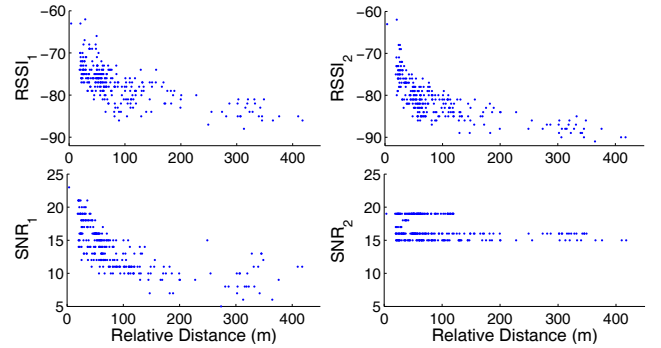


Figure 7: RSSIs and SNRs, antenна 1 (left) and 2 (right), vs. relative distance for Scenario B.

signal propagation at least half of the time. Conversely, the signal propagation is almost always partially obstructed by one UAV's body in Scenario B. (Note that the UAVs are flying at altitudes that are about 20 m apart.)

We observe that Scenario B shows a higher variability of RSSI and SNR (for instance, standard deviations of RSSI₁ and SNR₁ of Scenario A are respectively 3.486 and 2.256, while for Scenario B they are 4.435 and 3.364), but also more samples with better quality (higher RSSI and SNR). We can conclude that, despite the lower relative speed between the two UAVs in Scenario B (and thus lower impact of Doppler effect), the relative orientation of the antennas causes severe obstruction of the line-of-sight signal in this scenario, and consequently a degradation of the PDR.

5.2.4 Impact of PHY Rate

In the following, we further stress Scenario B, characterized by a relative speed between the UAVs equal to or smaller than 10 m/s for $\approx 97\%$ of the samples. We want to compare auto PHY rate adaptation with fixed PHY rate settings. Thus, we select representative modulation schemes and coding rates, which are differentiated by a Modulation and Coding Scheme (MCS) index value. In Figure 9, the different results for auto rate adaptation and the fixed PHY rate are shown for MCS index of 1 and 8. For both MCS tests, the supported fixed PHY rate is 30 Mb/s in the 40 MHz channel. The difference between them lies in the number of spatial streams supported; MCS1 supports one spatial stream, while MCS8 supports two spatial streams.

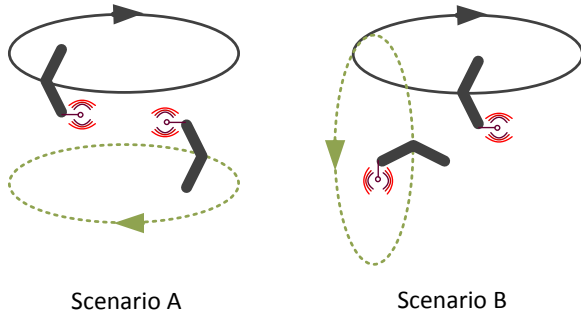


Figure 8: Antenna positions and trajectories.

As shown in Figure 9, the auto PHY rate results in less throughput compared to the static PHY rates for various ranges of distance (up to 300 m). In particular by fixing the PHY rate to MCS1, higher throughput is observed than for the adaptive PHY rate. The low performance figure of the auto-rate can be a consequence of the high mobility of UAVs. Since the rate adaptation implementation is open source, we expect that improvements are possible by making the algorithm aware of the relative distance between UAVs. Besides, in Figure 9 we see that one spatial stream (MCS1) outperforms the two spatial streams (MCS8). This is likely caused by the space-time encoding scheme of MCS1 which ensures a diversity gain at the receiver side. As a consequence, a higher quality of the received signal can be maintained.

5.2.5 Battery Consumption

To make a first attempt towards investigating energy consumption of aerial UAV communication, we enable tracking of energy readings. In every log entry, the battery level of a UAV is collected, which denotes the energy left for the entire system to operate and fly. Note that we do not have any on-board facility/sensor to accurately isolate power consumption of wireless communication from the overall power consumption.

Figure 10 visualizes the energy level for two traces of Scenario A and B. In both tests, wireless communication uses auto PHY rate. We observe a faster depletion of the battery for Scenario A. Considering the slope of a fitted line to Scenario A (with coefficient -0.0033) and comparing to that of Scenario B (with coefficient -0.0018), one can conclude that Scenario A drains the battery $\frac{-0.0033}{-0.0018} = 1.83$ times faster than Scenario B.

Among the possible reasons are the different cruise speed and wind speed during the experiments, but also the higher data rate permitted for Scenario A (80 Mb/s) with respect to the data rate of Scenario B (30 Mb/s). The lower data rate reduces the load of both the CPU and the WLAN chipset. We plan to investigate this phenomenon further in future work.

6. AERIAL TRANSMISSION

From our experiments, we can draw some conclusion on how long it would take to transmit image data. In the following investigations, we focus on the data collected in one cell (see Figure 1).

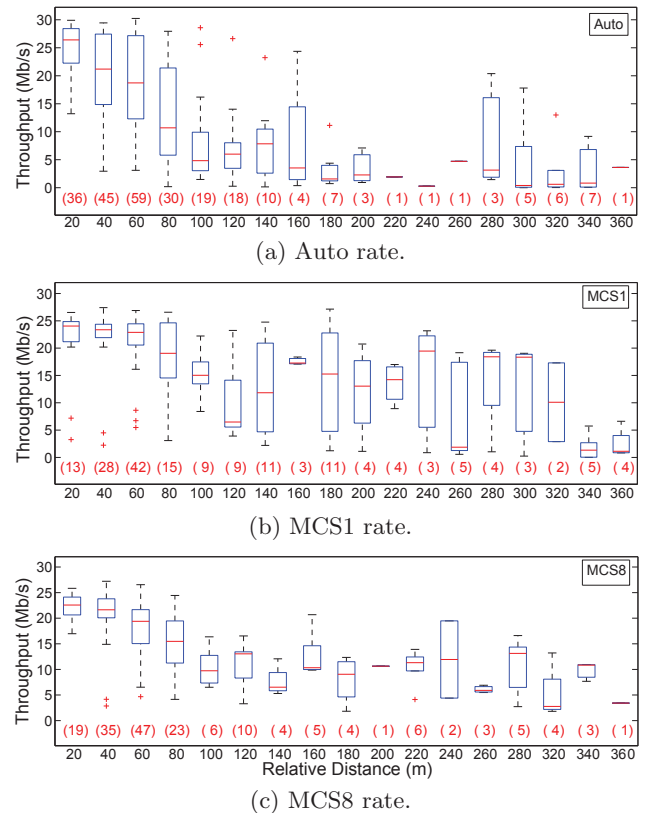


Figure 9: Throughput vs. distance for different PHY rate schemes, using Scenario B

6.1 Aerial Transmission Time

We define the *aerial transmission time* as the delay between the time the first packet of the set of images taken from the cell is in the head of the transmission queue and the instant when the last packet has been successfully delivered. The transmission time can be calculated from Little's law as:

$$T_{\text{transmission}} = \frac{\mathbb{E}[n_{\text{backlog}}]}{S/\mathbb{E}[P]} \cdot \frac{M_{\text{cell}}}{\mathbb{E}[P]} = \frac{\mathbb{E}[n_{\text{backlog}}] \cdot M_{\text{cell}}}{S}, \quad (2)$$

where S is the system throughput in bit/s, $\mathbb{E}[n_{\text{backlog}}]$ is the average number of UAVs within collision domain with backlog traffic, $\mathbb{E}[P]$ is the average amount of payload bits and M_{cell} is the total number of bits of the images collected in the cell. Hereby, we do not consider the probability that packets are dropped due to the limited number of 802.11n MAC retransmissions.

Due to losses and PHY rate adaption under mobility, 802.11n theoretical models may not be representative for actual throughput in an aerial network. Thus, we use our empirical data to fit a logarithmic function of base 2 [9] to the median values of the throughput versus distance measurements (with auto PHY rate):

$$\hat{S}(d, n_{\text{backlog}} = 1) = 10^6 \cdot (-6.142 \cdot \log_2(d) + 53.08). \quad (3)$$

This fitting results in a coefficient of determination, R^2 , equal to 0.95.

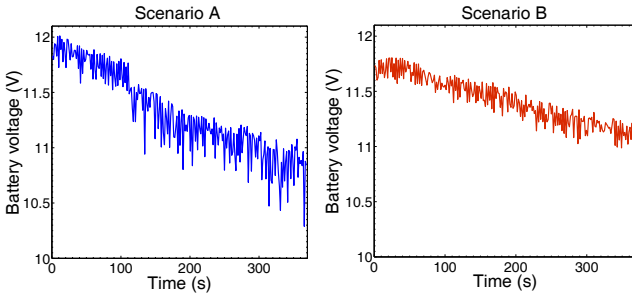


Figure 10: Battery consumption for a single trace of Scenario A and B.

6.2 Transmission Time versus Distance

Here, we study how the transmission time varies over distance. For reasons of simplicity, we assume that the delivery of data entirely occurs at a fixed distance. We use two different types of camera resolution, both with the aspect ratio $k = 16/9$. The size of the picture, M_{image} , is calculated using the JPEG100 format (100% quality, 24 bit/pixel) [6].

We compute the technical prerequisites sufficient to detect a person. Flying at an altitude of 70 m, and with camera lens angle of 65°, we get pictures with a field of view $\text{FOV} = 90$ m and an image area $A_{\text{image}} = 44 \times 78 = 3432 \text{ m}^2$. Table 2 summarizes the parameters. Hence, we compute M_{cell} using Equation (1) and $A_{\text{cell}} = 0.25 \text{ km}^2$.

Using Equation (2) and (3), the setting as above and the simple case of $\mathbb{E}[n_{\text{backlog}}] = 1$, Figure 11 shows the time needed to transmit the data with varying distances on a log scale, for both camera resolutions. One result, in particular for higher resolution images, is that due to the limitation of current 802.11n implementations for aerial transmissions, it takes several minutes to transmit reasonable amounts of image data to a UAV in range. This is a clear bottleneck for delivering high-resolution images. As a way to address this issue, scheduling algorithms which consider the spatial trajectory of the UAVs (and thus transmit when shorter distances are expected) may achieve considerable performance improvements.

7. CONCLUSION

While civil UAV applications benefit from the miniaturization of camera technology, delivering higher image quality, e.g., to rescuers also requires increased communication throughput. In indoor environments, such a technology already exists, i.e., 802.11n. Naturally, one may think to apply it to the drones for aerial communication. Yet, we have shown in real experiments that the achievable 802.11n throughput is not only far from the theoretical maximum – it also varies wildly even at similar distances between UAVs. Our measurements dedicated to determining the impact of relative node speed did not indicate a statistically signif-

Table 2: Aerial transmission parameters.

Camera resolution [pixel]	2664×1496	1280×720
M_{image} [MB]	1.2	0.390
M_{cell} [MB]	87	27.7

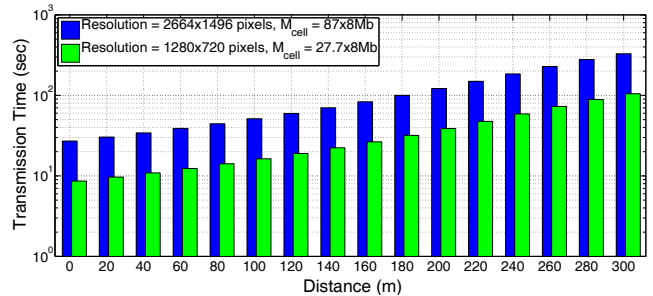


Figure 11: Aerial transmission time $T_{\text{transmission}}$ sending a set of images at a resolution of 2664×1496 and 1280×720 pixels to another flying UAV (log scale).

icant correlation of throughput and speed, but we found from medium to low loss rates across different relative cruise speeds. Yet, we learned that automatic rate adaptation of standard 802.11n chipsets cannot cope with the high mobility of UAVs, and that UAV’s antenna position is crucial to guarantee the expected quality of communication. These and other results of this contribution require further scientific investigation, yet, they indicate the need for a new amendment of 802.11 to assure the high-speed and reliable communication between UAVs that is required in order not to limit the immense potential of drones.

8. ACKNOWLEDGMENTS

The authors would like to greatly thank Maja Varga and Gregoire Heitz of EPFL for their support during in-flight tests and Dr. Simon Heimlicher for multiple discussions. We are finally thankful to Prof. Mahesh Marina from The University of Edinburgh for insightful comments in the preparation of the camera ready version of the paper. This research has been partially funded by the Swiss National Science Foundation (SNSF) Sinergia project SWARMMIX, with project number CRSI22_133059 and by the Commission of the European Union under the FP7 Marie Curie IEF program contract PIEF-GA-2010-276336 MOVE-R.

9. REFERENCES

- [1] IEEE standard for information technology – telecommunications and information exchange between systems local and metropolitan area networks – specific requirements part 11: Wireless LAN medium access control (MAC) and physical layer (PHY) specifications, 2012.
- [2] D. Aguayo, J. Bicket, S. Biswas, G. Judd, and R. Morris. Link-level measurements from an 802.11b mesh network. *ACM SIGCOMM Computer Communication Review*, 34(4):121–132, 2004.
- [3] M. Asadpour, D. Giustiniano, K. A. Hummel, and S. Heimlicher. Characterizing 802.11n aerial communication. In *Proceedings of the second ACM MobiHoc workshop on Airborne networks and communications*, ANC ’13, pages 7–12, New York, NY, USA. ACM, 2013.
- [4] L. Duplay. Target detection using flying robots. Technical report, Laboratory of Intelligent Systems (LIS), EPFL, June 2012.

- [5] E. Feo, L. Gambardella, and G. D. Caro. Search and rescue using mixed swarms of heterogeneous agents: Modeling, simulation, and planning. Technical Report IDSIA-05-12, April 2012.
- [6] P. Forret. Megapixel Calculator - digital camera resolution. <http://web.forret.com/tools/megapixel.asp>.
- [7] J. Heiskala and J. Terry. *OFDM wireless LANs: a theoretical and practical guide*. SAMS publishing Indianapolis, 2002.
- [8] D. Henkel and T. Brown. On controlled node mobility in delay-tolerant networks of unmannned aerial vehicles. In *International Symposium on Advance Radio Technologies*, 2006.
- [9] D. Henkel and T. Brown. Delay-tolerant communication using mobile robotic helper nodes. In *Modeling and Optimization in Mobile, Ad Hoc, and Wireless Networks and Workshops, 2008. WiOPT 2008. 6th International Symposium on*, pages 657–666. IEEE, 2008.
- [10] O. Küng, C. Strecha, A. Beyeler, J.-C. Zufferey, D. Floreano, P. Fua, and F. Gervais. The accuracy of automatic photogrammetric techniques on ultra-light uav imagery. In *Proceedings of the International Conference on Unmanned Aerial Vehicle in Geomatics (UAV-g)*, Zurich, Switzerland, pages 14–16, 2011.
- [11] S. Leven, J. Zufferey, and D. Floreano. A simple and robust fixed-wing platform for outdoor flying robot experiments. In *International symposium on flying insects and robots*, pages 69–70, 2007.
- [12] L. Meier, P. Tanskanen, L. Heng, G. H. Lee, F. Fraundorfer, and M. Pollefeys. Pixhawk: A micro aerial vehicle design for autonomous flight using onboard computer vision. *Autonomous Robots*, 33(1-2):21–39, 2012.
- [13] K. Pelechrinis, T. Salonidis, H. Lundgren, and N. Vaidya. Experimental characterization of 802.11n link quality at high rates. In *Fifth ACM international workshop on Wireless network testbeds, experimental evaluation and characterization, WiNTECH ’10*, pages 39–46, New York, NY, USA. ACM, 2010.
- [14] T. Rappaport. *Wireless Communications: Principles and Practice*, 2nd Ed. Prentice Hall, New Jersey, 2002.
- [15] V. Shrivastava, S. Rayanchu, J. Yoonj, and S. Banerjee. 802.11n under the microscope. In *8th ACM SIGCOMM conference on Internet measurement*, pages 105–110. ACM, 2008.
- [16] I. Tinnirello, D. Giustiniano, L. Scalia, and G. Bianchi. On the side-effects of proprietary solutions for fading and interference mitigation in IEEE 802.11b/g outdoor links. *Computer Networks*, 53(2):141–152, Feb. 2009.
- [17] E. Yanmaz, R. Kuschnig, and C. Bettstetter. Channel measurements over 802.11 a-based uav-to-ground links. In *GLOBECOM 2011 Workshops*, pages 1280–1284. IEEE, 2011.
- [18] E. Yanmaz, R. Kuschnig, and C. Bettstetter. Achieving air-ground communications in 802.11 networks with three-dimensional aerial mobility. In *INFOCOM 2013. 32nd IEEE International Conference on Computer Communications*, pages 120–124. IEEE, 2013.
- [19] W. Zhao, M. Ammar, and E. Zegura. Controlling the mobility of multiple data transport ferries in a delay-tolerant network. In *INFOCOM 2005. 24th Annual Joint Conference of the IEEE Computer and Communications Societies*, volume 2, pages 1407–1418. IEEE, 2005.